MALDI-TOF/TOF Tandem Mass Spectrometry Imaging Reveals Non-uniform Distribution of Disaccharide Isomers in Plant Tissues

Lingpeng ZHAN[ab], Xi HUANG[ab], Jinjuan XUE[ab], Huihui LIU[a], Caiqiao XIONG[a]*, Jiyun WANG[a], and Zongxiu NIE[ac]*

[a] Beijing National Laboratory for Molecular Sciences, Key Laboratory of Analytical Chemistry for Living Biosystems, Institute of Chemistry, Chinese Academy of Sciences, Beijing 100190, China

[b] University of Chinese Academy of Sciences, Beijing 100049, China

[c] National Center for Mass Spectrometry in Beijing, Beijing 100190, China

Email: lingpengfir@126.com; 1100011767@pku.edu.cn; xuejinjuan@iccas.ac.cn; hhliu@iccas.ac.cn; xiongcq@iccas.ac.cn; znie@iccas.ac.cn

*Corresponding author. Z.Nie, email: znie@iccas.ac.cn; telephone: 0086-010-62652123;

C.Xiong, email: xiongcq@iccas.ac.cn, telephone: 0086-010-82612849

Abstract

Mass spectrometry imaging (MSI) is powerful for investigating the biomolecular locations within tissues. However, the isomeric compounds are rarely distinguished due to inability of MSI to differentiate isomers in the probing area. Coupling tandem mass spectrometry with MSI can facilitate differentiating isomeric compounds. Here we apply MALDI-TOF/TOF tandem mass spectrometry imaging approach to revealing the spatial distributions of isomeric disaccharides in plant tissues. First, the MS/MS imaging analysis of disaccharide-matrix droplet spots demonstrated the feasibility of distinguishing isomeric species in tissues, by measuring the relative intensity of specific fragments. Then, we conducted tandem MS imaging of disaccharides in onion bulb tissues, which indicated that sucrose and other unknown non-sucrose disaccharides exhibit heterogeneous locations throughout the tissues. This method enables us to image disaccharide isomers differentially in biological tissues, and to discover new saccharide species in plant. This work also emphasizes the necessity of considering isobaric compounds when interpreting MSI results.

Keywords: MALDI-TOF; tandem mass spectrometry imaging; disaccharide isomer; onion bulb; sucrose;

Introduction

Mass spectrometry imaging (MSI) has become more and more popular in visualizing metabolites (Banerjee, Zare, Tibshirani, Kunder, Nolley, Fan, et al., 2017), lipids (Ellis, Paine, Eijkel, Pauling, Husen, Jervelund, et al., 2018), proteins (Garza, Feider, Klein, Rosenberg, Brodbelt, & Eberlin, 2018) and even nanomaterials (Chen, Xiong, Liu, Wan, Hou, He, et al., 2015; Xue, Liu, Chen, Xiong, Zhan, Sun, et al., 2018) in biological samples, including plant tissues (Liao, Fu, Zhou, Rao, Zeng, & Yang, 2019). The distribution of biomolecules can provide valuable information on the growth and physiological status of plants (Peukert, Thiel, Peshev, Weschke, Van den Ende, Mock, et al., 2014; Shroff, Vergara, Muck, Svatos, & Gershenzon, 2008). However, there is a significant issue in MSI analysis that isobaric species in the same position could not be differentiated, which may cause the misinterpretation of location and function of isomers. This limitation could be overcome by coupling MSI with approaches capable of resolving the isobaric molecules, such as ion mobility (Nagy, Velickovic, Chu, Carrell, Weston, Ibrahim, et al., 2019; Sans, Feider, & Eberlin, 2018) and tandem mass spectrometry (Fu, Touboul, Della-Negra, Houel, Amusant, Duplais, et al., 2018). For example, MS/MS imaging of lipid phosphatidylglycerol (PG) 34:3 in the maize leaves showed that isomeric lipids PG (18:3/16:0) and PG (18:2/16:1) have divergent locations, which might be neglected in MS imaging (Duenas, Klein, Alexander, Yandeau-Nelson, Nikolau, & Lee, 2017). The observation that isomeric molecules have different distributions was also found in other plant tissue. For instance, MS images of *m/z* 1319 was drastically different from the MS/MS images of *m/z* 1319→1247 and *m/z* 1319→995 in Populus tissue (Lunsford, Peter, & Yost, 2011). However, most of the tandem MS imaging aims at eliminating the interference from matrix, thus facilitating the target and quantification analysis of small molecules (Porta, Grivet, Kraemer, Varesio, & Hopfgartner, 2011). Moreover, tandem MS imaging would be practicable only in the case that the MS/MS of isobaric precursors generate different fragment ions. Unfortunately, some isomers are not easily discriminated by tandem mass spectrometry as a standalone methodology, such as glycan and lipid isomers. Carrying out chemical reaction with isomers before MS^2 can be helpful for discriminating them in the tandem mass spectra. Recent efforts in coupling special reaction to tandem mass spectrometry imaging have succeeded in discriminating isomeric lipids in the same probed tissues, such as on-tissue Paterno-Buchi reaction (Bednarik, Bolsker, Soltwisch, & Dreisewerd, 2018; Waldchen, Spengler, & Heiles, 2019) and ozone-induced dissociation (Paine, Poad, Eijkel, Marshall, Blanksby, Heeren, et al., 2018). Another strategy to tackling the isomeric issue in MSI is to separate isomers before sampling, that is, utilizing structure-specific derivatization methods to modify one of the isomers. For example, the linkage-specific in situ derivatization of sialic acid have been performed before MSI to separate the 2,3-sialyllactose and 2,6-sialyllactose in tissues (Holst, Heijs, de Haan, van Zeijl, Briaire-de Bruijn, van Pelt, et al., 2016). However, structure-specific reactions are rarely available.

Mapping the disaccharide over time and space provide important implications for understanding the adaptive and stress response (Guendel, Rolletschek, Wagner, Muszynska, & Borisjuk, 2018). Moreover, the distribution of carbohydrates can serve as indicators for the flavor of fruits. One MSI study found that sucrose are mainly distributed in the upper side of cortical and pith tissue, which indicated top side are sweeter than bottom side of strawberry (Enomoto, Sato, Miyamoto, Ohtsuka, & Yamane, 2018; Guendel, Rolletschek, Wagner, Muszynska, & Borisjuk, 2018). In some reports, the disaccharides in some plant tissues were merely assigned to sucrose, such as Medicago (Ye, Gemperline, Venkateshwaran, Chen, Delaux, Howes-Podoll, et al., 2013), cassava tuber (Li, Knudsen, Hansen, Jorgensen, Kannangara, Bak, et al., 2013), and soybean seeds (Sagara, Bhandari, Spengler, & Vollmann, 2020). However, other disaccharide isomers

should also be considered. For example, only sucrose was identified in Medicago in a previous MSI study (Ye, et al., 2013), while both sucrose and maltose were detected in Medicago by our recent MS/MS study (Zhan, Xie, Li, Liu, Xiong, & Nie, 2018).

In this work, we demonstrate that MALDI-TOF/TOF tandem mass spectrometry imaging can reveal the divergent distribution of disaccharide isomers in plant tissues. In our previous work, we showed that disaccharide isomers can be differentiated and relatively quantified by the characteristic fragments produced by MALDI-TOF/TOF in the negative mode. We further extend this approach to monitoring the fragments of disaccharide-chloride adduct $[M+Cl]^-$ throughout the plant tissue. We showed that MS/MS imaging can distinguish sucrose and non-sucrose disaccharides within the same plant tissue and lead to discovering new disaccharide species in onion bulb.

Materials and Methods

Chemical and Materials

Chemicals. N-(1-naphthyl) ethylenediamine dihydrochloride (NEDC) and maltose were purchased from Sigma-Aldrich (St. Louis, MO, U.S.A.). Acetonitrile (HPLC grade), ethanol (HPLC grade) and methanol (HPLC grade) were obtained from Thermo Fisher. The water was prepared using a Milli-Q water purification system (Millipore, MA, USA). The disaccharides isomaltose was obtained from TCI (Tokyo, Japan). Cellobiose was from J&K (Beijing, China). Melibiose was purchased from Aladin (Beijing, China). All the disaccharide standards were dissolved in water at 100 μmol/L.

Plant tissues

Plant samples were purchased from local supermarket in Beijing. First, the plants, that is purple onion, white onion, purple grape and green grape, were flash-frozen in liquid N_2, and then incubated in -20°C refrigerator for several hours. Next, the plant samples were sectioned at 20 μm thickness using a Leica CM1950 cryostat (Leica Microsystems GmbH, Wetzlar, Germany) at −20°C and thaw mounted onto indium tin oxide (ITO) coated glass slides. Extracts of onion bulb tissue was prepared in 50% water/methanol for 8 hrs.

Mass spectrometry imaging

For MS and tandem MS imaging, NEDC (6 mg/mL) in 50% ethanol/water prepared was sprayed onto the tissue sections using automatic matrix sprayer (ImagePrep, Bruker Daltonics, Germany). The key parameters of ImagePrep in these experiments are as follows: number of cycle, 35; spray power, 62%; spray modulation, 15%; spray on, 1 s; incubation, 20 s; dry time, 75 s. MS and MS/MS imaging were performed on an MALDI-TOF/TOF mass spectrometer (Ultraflextreme, Bruker Daltonics, Germany) equipped with a smartbeam Nd:YAG laser source (355 nm, 2 kHz). The MS and tandem MS imaging were operated in the negative mode. The laser power was set at 40%, repetition rate was 1 kHz. MS and MS/MS imaging spatial resolution were set to 200 μm. Each pixel was accumulated of 200 laser shots. Regions of imaging were defined by using the optical image and MSI data image. For tandem MSI, LIFT spectra of *m/z* 377 (selection window was set at ±3 Da) were monitored across the whole tissue. The imaging data were acquired and processed using FlexImaging 3.0 (Bruker Daltonics, Germany).

Results and discussion

Tandem MS imaging for differentiating disaccharide isomers

Coffee ring effect is a common phenomenon found in dried droplet spot (Hu, Chen, & Urban, 2013), which can cause trouble for the quantitative analysis of biomolecules by MALDI-MS. In our previous report, we successfully quantified the disaccharide isomers in a binary mixture based on their characteristic fragment ions (Zhan, Xie, Li, Liu, Xiong, & Nie, 2018), and applied this method to the detection of honey adulteration recently (Qu, Jiang, Huang, Cui, Ning, Liu, et al., 2019). However, an important prerequisite proposed that the coffee ring or sweet spot phenomenon would not affect the performance of quantitative analysis, which means that the ratios of characteristic fragments are very similar throughout the whole dried spot. There was very little variation of fragment ratios between measurements of eight different probed positions within one spot (Zhan, Xie, Li, Liu, Xiong, & Nie, 2018). To test this hypothesis, we performed MS/MS imaging of precursor ion *m/z* 377 ($[M + Cl]^-$, M is the molecule of disaccharide and has a mass of 342) of four dried droplet spots of disaccharide isomers (i.e. isomaltose, cellobiose, maltose and melibiose) with matrix. As shown in Figure 1a, we observed that most signals of fragment *m/z* 281 were found in the rim of spot when the ion images were not normalized. However, when the images were normalized to total ion current (TIC), we found that fragment *m/z* 281 ($[M-H-60]^-$) formed homogeneous distribution in those spots, as shown in Figure 1b. Based on these observation, we can see that the relative intensity of *m/z* 281 are stable across different positions within the whole spot. It's worth noting that the "relative intensity" we used here doesn't mean exact relative intensity of a fragment compared to most intensive peak in one mass spectrum, because of the normalization method in MSI (Deininger, Cornett, Paape, Becker, Pineau, Rauser, et al., 2011). We normalize the ion image to TIC in this work. Because we only monitor the fragments of ion *m/z* 377 in this work, most ions appeared in spectra are fragments of disaccharides and thus TIC is summation of all fragment ions in all probed positions. The color of a fragment in normalized MS/MS images can represent its fraction in all fragments. Meanwhile, all four disaccharide-matrix spots showed similar phenomenon by comparing the images after two data processing methods, as shown in Figure 1a and 1b. Moreover, the diverse colors of ion images of four disaccharide isomer spots indicated that the relative abundance of *m/z* 281 were different in these tandem mass spectra, and thus could also be used to differentiate these isomers. The representative MS/MS spectra in the center (up panel) and rim (down panel) of the maltose-matrix spots are displayed in Figure 1c. The signals (ordinate value) of fragments were much stronger in the rim than that in the center region, due to the "coffee ring effect". Though there are significant difference between the absolute intensity of fragment ions in these regions, we found no obvious difference between their fragment patterns. These results demonstrated that the MS/MS imaging can be used to reflect the diverse distribution of disaccharide isomers, by comparing the relative intensity of certain fragment ion, despite that they have same fragment species. To further validate the method, we prepared mixture of isomaltose and maltose in different ratios and imaged the droplet spots in the MS/MS mode. As shown in Figure S1, the color of ion images of *m/z* 161 changed gradually with increasing quantity of maltose. When the ratio of isomaltose to maltose changed from 5:1 to 1:5, the ion images of *m/z* 161 changed from blue (Figure S1a) to red (Figure S1d). Meanwhile, the ratio of *m/z* 161 to 179 in the extracted mass spectra changed from 11:100 (Figure S1a) to 100:83 (Figure S1d). This observation is consistent with our previous measurements (Zhan, Xie, Li, Liu, Xiong, & Nie, 2018).

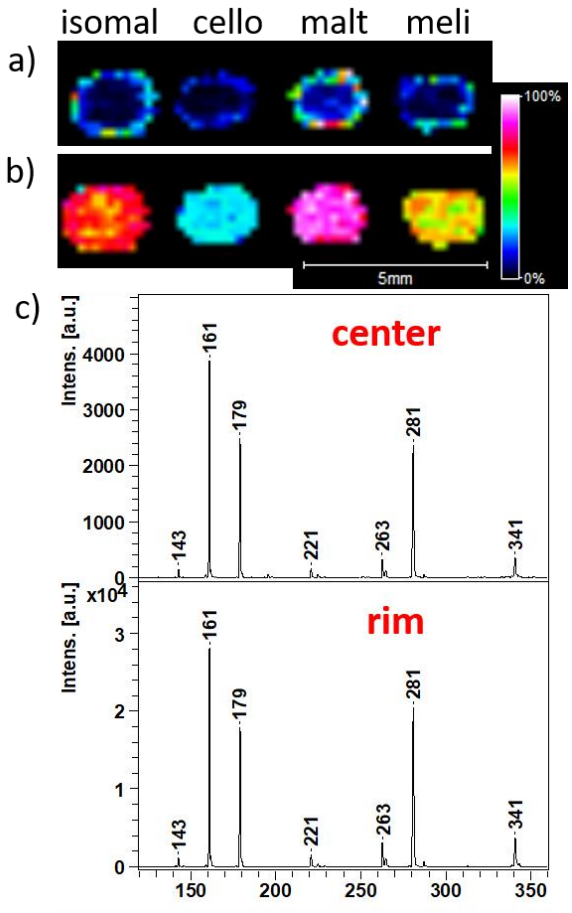

Figure 1 MALDI-MS/MS imaging of disaccharide-matrix mixture spots. The ion images of fragment *m/z* 281 of disaccharide isomers were displayed, from left to right: isomaltose, cellobiose, maltose, melibiose, respectively. The images were processed as a) no normalization and b) normalized to TIC. c) Representative MS/MS spectra of maltose in the center (up) and rim (bottom) of the dried spot.

MS and MS/MS imaging of purple onion bulb

Disaccharides are important energy sources (carbohydrate energy storage molecule) utilized by biological systems, for example sucrose for plant and trehalose for microorganisms (Ye, et al., 2013). Moreover, some disaccharides have particular bio-functions, other than energy storage (Jensen, Peters, & Bhuvaneswari, 2002; Paz-Alfaro, Ruiz-Granados, Uribe-Carvajal, & Sampedro, 2009). To better understand the roles of disaccharides in plant, we investigated the spatial distribution of disaccharides in various plants, including onion and grape, by recording the TOF/TOF spectra of *m/z* 377 throughout the tissue. Before that, we have applied mass spectrometry imaging to mapping the distributions of some biomolecules within purple onion bulb tissue. The MSI result indicated that some compounds exhibit distinct locations within onion bulb cross section, as shown in Figure 2. The optical photo of onion bulb tissue is displayed in Figure 2a, indicating the outer epidermis with purple rim. For example, trisaccharide ions $[DP3+Cl]^-$ (*m/z* 539) and disaccharides ions $[DP2+Cl]^-$ (*m/z* 377) were mostly detected in the inner epidermis (Figure 2b), while flavone derivatives *m/z* 625 ($C_{27}H_{30}O_{17}(-H^+)$) and *m/z* 463 ($C_{21}H_{20}O_{12}(-H^+)$) were found in the outer epidermis cells (Figure 2c). It revealed that the compounds in the outer epidermal cell and inner epidermal cell of purple onion (*A. cepa*) bulb are different, which had also been

demonstrated by single cell mass spectrometry analysis (Gong, Zhao, Cai, Fu, Yang, Zhang, et al., 2014). Our MSI results is consistent with the single cell MS measurements, indicating that inner epidermis has more glycans than outer epidermis cells. Moreover, the single cell analysis estimated the sucrose concentration to be 20-50 mM, but the authors did not take other disaccharide isomers into consideration.

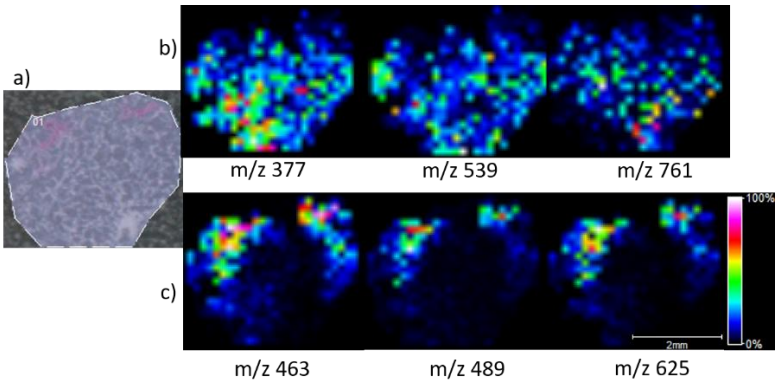

Figure 2 Mass spectrometry imaging of purple onion (A.cepa) bulb cross section. a) Optical photography of the onion cross-section. b) Ion images of molecules accumulating in the inner layer of onion revealed by MSI. c) Ion images of molecules accumulated in the outer layer of onion are revealed by MSI.

Next, we monitored the fragments of disaccharide chloride adduct $[M+Cl]^-$ (*m/z* 377) throughout the onion bulb tissue in the TOF/TOF imaging mode. The normalized ion images of several fragments were displayed in Figure 3b and 3c. Obviously, the product ions *m/z* 215 ($[M-C_6H_{10}O_5+Cl]^-$) and 341 ($[M-H]^-$) are accumulated in inner epidermis of onion bulbs (Figure 3a and 3c), while fragment ions *m/z* 251 ($[M-H-C_3H_6O_3]^-$), 281 ($[M-H-C_2H_4O_2]^-$), 161 ($[M-H-C_6H_{12}O_6]^-$), 179 ($[M-H-C_6H_{10}O_5]^-$) and 221 ($[M-H-C_4H_8O_4]^-$) are mainly found in the middle epidermis region (Figure 3b). The phenomenon observed in the non-normalized images were similar with that in the normalized ones (Figure S2). In our previous report, we confirmed the existence of sucrose from the diagnostic peaks of *m/z* 215 and 341 (Zhan, Xie, Li, Liu, Xiong, & Nie, 2018). In this work, we also assigned these peaks to the presence of sucrose in onion bulb, which have also been determined by GC (gas chromatography) and LC (liquid chromatography) (Benkeblia, Onodera, & Shiomi, 2004; Davis, Terry, Chope, & Faul, 2007; Downes & Terry, 2010). However, identifying other disaccharide isomers is not easy because the possibility of coexisting multi-isomers. We suggest that chemical derivatization coupled with GC-MS and LC-MS could identify these disaccharides, by comparing them with disaccharide standards as possible candidates (Liu, Lou, Ding, Li, Qi, Zhu, et al., 2013; Pokrzywnicka & Koncki, 2018). The representative tandem mass spectra of disaccharides in the middle and inner epidermis region were shown in Figure 3d and 3e, respectively. Clearly, their mass spectra were different from each other, especially the relative abundance of *m/z* 179 ($[M-H-163]^-$) and 341 ($[M-H]^-$). Based on above discussion, the difference of fragmentation pattern indicated the different compositions of disaccharides in these regions. To validate these observations, we cut the onion bulb into halves and extracted carbohydrates with 50% methanol solution. The tandem mass spectra of disaccharides in the extracts are shown in Figure S3. The MS/MS results were in accordance with that in the TOF/TOF imaging,

indicating that there was no or few delocalization of glycans during sectioning bulb tissue. The lateral resolutions of these images are relatively lower than some published animal tissue, due to intrinsic characters of plant tissue, such as complex texture, low lipid and high water content (He, Guo, Luo, Sun, Lin, & Cai, 2019; Li, Zhang, Ge, Liu, & Li, 2018). Since most studies of the disaccharide in onion was on sucrose (Benkeblia, Onodera, & Shiomi, 2004; Pohnl, Schweiggert, & Carle, 2018), our findings demonstrated the presence of other disaccharide isomers and they exhibited distinct distributions within onion bulb. The observation here was also found in another purple onion bulb tissue (Figure S4), exclude the possibility of artificial results. In a previous report, the distribution of linkage and anomeric isomers of disaccharide was investigated in a tripartite symbiosis system of moss, cyanobacteria, and fungus in the positive mode (Velickovic, Chu, Carrell, Thomas, Pasa-Tolic, Weston, et al., 2018). We believe that our method can also be applied in the bio-system of plant-fungus symbiosis.

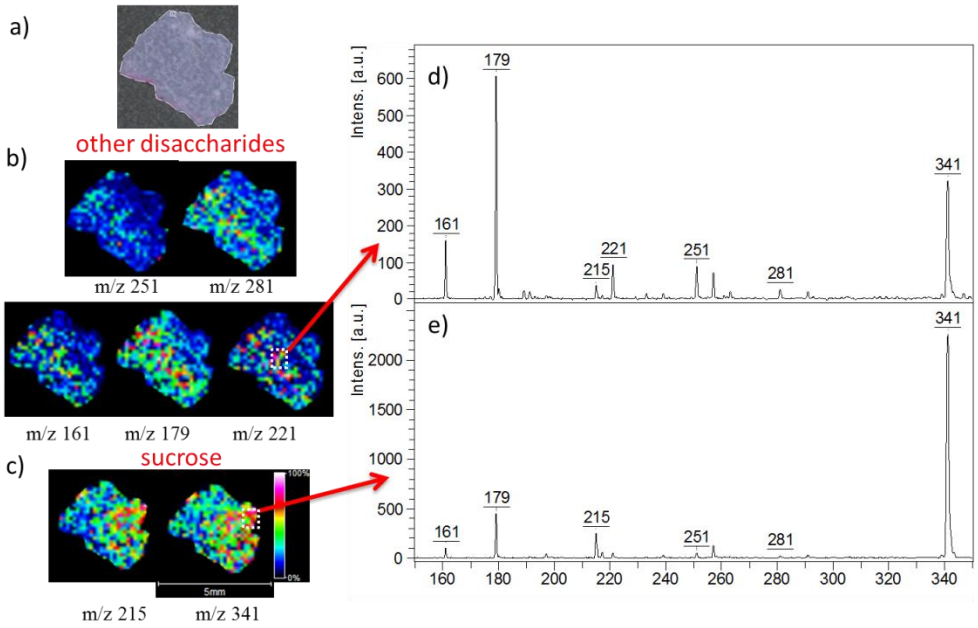

Figure 3 MALDI-TOF/TOF imaging of disaccharide isomers in purple onion bulbs. a) optical photography of onion bulb tissue, outer epidermis is in left bottom with red edge; b) the ion images of fragments derived from non-sucrose disaccharides; c) the ion images of fragments *m/z* 215 and 341, which derived from sucrose; d) the representative mass spectrum of region with dominant non-sucrose disaccharides; e) representative mass spectrum of region with dominant sucrose signals. The ion images were normalized to TIC. All the ion images have same full intensity threshold in color bar.

MS/MS imaging of disaccharides in other plant tissues

Furthermore, we performed the tandem mass spectrometry imaging analysis of disaccharides in other plant tissue, namely, white onion and grape. We compared the MS imaging and MS/MS imaging results of white onion bulb cross section, as shown in Figure 4. From the ion image of *m/z* 377, we found that the distribution of disaccharides was homogenous across the tissue, without an

obvious uneven distribution in different regions of bulb tissue. However, ion images of fragment *m/z* 161 show distinct distribution in the bulb cross section, implying that non-sucrose disaccharides accumulate in the outer epidermis region.

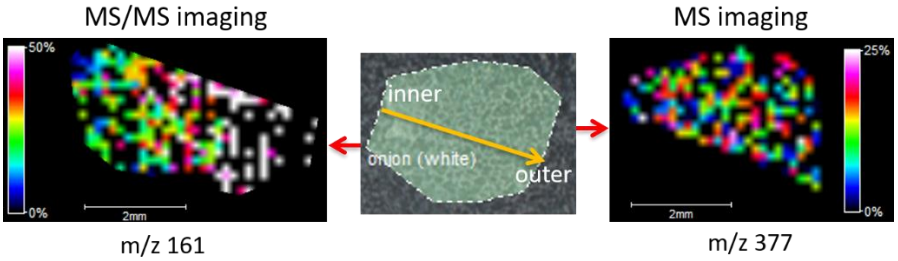

Figure 4 Comparison of the MS/MS imaging and MS imaging of disaccharides in the white onion bulb cross section. MS imaging reveals a homogenous distribution of disaccharides, but the MS/MS image shows that sucrose relatively accumulated in the inner layer. The yellow arrow points from inner epidermis to the outer epidermis. MS/MS image was normalized to TIC. Different maximum intensity thresholds were applied in these two images.

When comparing the ion images of fragments *m/z* 215 and 161, we observed an interesting phenomenon that the relative intensity of *m/z* 215 and 161 gradually changed across the tissue. It indicates that the proportion of sucrose (*m/z* 215) in total disaccharides decreased gradually from inner epidermis to outer epidermis region, as shown in Figure 5a. On the contrary, the proportion of non-sucrose disaccharide isomer (*m/z* 161) increased gradually from inner epidermis to outer epidermis regions (Figure 5b). We divided the tissue into three parts, region of interest (ROI) 1 to 3, from left to right. The representative mass spectra of three ROIs are shown in Figure 5c, d and e, respectively. We found that the ratio of *m/z* 179 (or *m/z* 161) and 215 increased gradually from ROI 1 toward ROI 3. We observed a similar trend of fragment patterns in the ion images without normalization, as shown in Figure S5. This observation was slightly different from that in purple onion bulbs. A repeated experiment on another white onion bulb tissue showed similar phenomenon (Figure S6). In order to validate such distribution of disaccharide isomers, we have cut the white onion bulb and acquired the MS/MS spectra, in a same way with purple onion. The results also showed that inner epidermis have higher fraction of sucrose (Figure S7). Moreover, we also observed heterogeneous distribution of disaccharide isomers in purple (Figure S8) and green grape (Figure S9) cross sections.

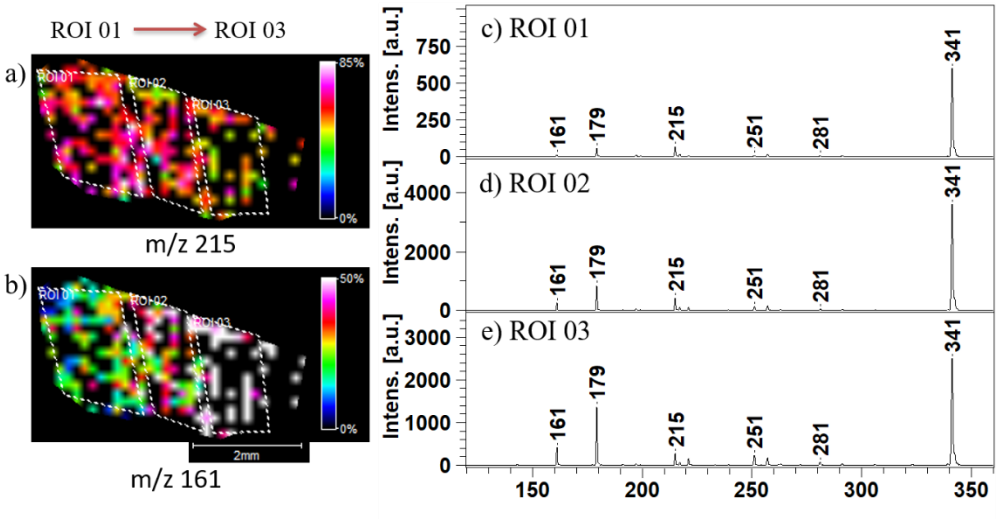

Figure 5 MALDI-TOF/TOF imaging of disaccharides in white onion; a) ion images of *m/z* 215; b) ion images of *m/z* 161; representative mass spectra of ROI were shown in c) ROI 01, b) ROI 02, e) ROI 03. ROI 01 was in the inner epidermis while ROI 03 was in the outer epidermis. The ion images are normalized to TIC. Different maximum intensity thresholds were applied in these two ion images.

In conclusion, we developed a tandem mass spectrometry imaging approach to map the distribution of disaccharide isomers in plant tissues. We demonstrated that isomers can be distinguished in the same tissue via MALDI-TOF/TOF tandem MSI. The experiments on plant tissue indicated the distinct distribution of sucrose and non-sucrose disaccharides. Such a distinct distribution of disaccharide isomers may suggest their diverse biological function, such as serving as carbon source, regulating protein function and so on. Infrared-based microspectroscopic method have also been utilized in visualizing sucrose distribution in the cereal crop barley and Arabidopsis, but it can't distinguish sucrose from other disaccharide isomers (Guendel, Rolletschek, Wagner, Muszynska, & Borisjuk, 2018). Comparing with the recent report utilizing liquid extraction surface analysis (LESA)-ion mobility mass spectrometry in imaging disaccharide isomers (Nagy, et al., 2019), MALDI-TOF/TOF imaging is superior in lateral resolution and convenience, which could facilitate the study of bacteria-plant interaction in more details. However, for better interpreting the observation, we may need to include other analytical approaches (such as GC, LC and electrophoretic techniques) to identify the disaccharide isomers, by comparing the disaccharide standards and the disaccharides in plant extracts (Pokrzywnicka & Koncki, 2018). We believe that the plant physiologist and food chemist can benefit from our findings. For example, this method can be applied to investigate the effect of storage condition on distribution of saccharide within onions (Benkeblia, Onodera, & Shiomi, 2004). Recently, one study combining combined on-tissue chemical derivatization and tandem mass spectrometry imaging has revealed distinct distribution of steroid structural isomers in human adrenal glands (Takeo, Sugiura, Uemura, Nishimoto, Yasuda, Sugiyama, et al., 2019). This work suggests the significance of tandem mass spectrometry imaging in differentiating isomers of biological tissues. Our work also reminds of the mass spectrometry imaging community that even though fragment species of isomers are same, we can differentiate them in tissue by using relative intensity of definitive fragments.

Acknowledgments

This work was supported by grants from the National Natural Sciences Foundation of China (Grant Nos. 21625504, 21827807, 21675160, and 21790390/21790392), and Chinese Academy of Sciences.

Conflict of Interest Disclosure

The authors declare no conflict of interest.

228 REFERENCES

229 Banerjee, S., Zare, R. N., Tibshirani, R. J., Kunder, C. A., Nolley, R., Fan, R., Brooks, J. D., & Sonn, G.
230 A. (2017). Diagnosis of prostate cancer by desorption electrospray ionization mass spectrometric
231 imaging of small metabolites and lipids. *Proc Natl Acad Sci U S A, 114*(13), 3334-3339.
232 Bednarik, A., Bolsker, S., Soltwisch, J., & Dreisewerd, K. (2018). An On-Tissue Paterno-Buchi
233 Reaction for Localization of Carbon-Carbon Double Bonds in Phospholipids and Glycolipids by
234 Matrix-Assisted Laser-Desorption-Ionization Mass-Spectrometry Imaging. *Angew Chem Int Ed*
235 *Engl, 57*(37), 12092-12096.
236 Benkeblia, N., Onodera, S., & Shiomi, N. (2004). Effect of gamma irradiation and temperature on
237 fructans (fructo-oligosaccharides) of stored onion bulbs Allium cepa L. *Food Chem, 87*(3), 377-
238 382.
239 Chen, S., Xiong, C., Liu, H., Wan, Q., Hou, J., He, Q., Badu-Tawiah, A., & Nie, Z. (2015). Mass
240 spectrometry imaging reveals the sub-organ distribution of carbon nanomaterials. *Nat*
241 *Nanotechnol, 10*(2), 176-182.
242 Davis, F., Terry, L. A., Chope, G. A., & Faul, C. F. (2007). Effect of extraction procedure on measured
243 sugar concentrations in onion (Allium cepa L.) bulbs. *J Agric Food Chem, 55*(11), 4299-4306.
244 Deininger, S. O., Cornett, D. S., Paape, R., Becker, M., Pineau, C., Rauser, S., Walch, A., & Wolski, E.
245 (2011). Normalization in MALDI-TOF imaging datasets of proteins: practical considerations.
246 *Anal Bioanal Chem, 401*(1), 167-181.
247 Downes, K., & Terry, L. A. (2010). A new acetonitrile-free mobile phase method for LC-ELSD
248 quantification of fructooligosaccharides in onion (Allium cepa L.). *Talanta, 82*(1), 118-124.
249 Duenas, M. E., Klein, A. T., Alexander, L. E., Yandeau-Nelson, M. D., Nikolau, B. J., & Lee, Y. J.
250 (2017). High spatial resolution mass spectrometry imaging reveals the genetically programmed,
251 developmental modification of the distribution of thylakoid membrane lipids among individual
252 cells of maize leaf. *Plant J, 89*(4), 825-838.
253 Ellis, S. R., Paine, M. R. L., Eijkel, G. B., Pauling, J. K., Husen, P., Jervelund, M. W., Hermansson, M.,
254 Ejsing, C. S., & Heeren, R. M. A. (2018). Automated, parallel mass spectrometry imaging and
255 structural identification of lipids. *Nat Methods, 15*(7), 515-518.
256 Enomoto, H., Sato, K., Miyamoto, K., Ohtsuka, A., & Yamane, H. (2018). Distribution Analysis of
257 Anthocyanins, Sugars, and Organic Acids in Strawberry Fruits Using Matrix-Assisted Laser
258 Desorption/Ionization-Imaging Mass Spectrometry. *J Agric Food Chem, 66*(19), 4958-4965.
259 Fu, T., Touboul, D., Della-Negra, S., Houel, E., Amusant, N., Duplais, C., Fisher, G. L., & Brunelle, A.
260 (2018). Tandem Mass Spectrometry Imaging and in Situ Characterization of Bioactive Wood
261 Metabolites in Amazonian Tree Species Sextonia rubra. *Anal Chem, 90*(12), 7535-7543.
262 Garza, K. Y., Feider, C. L., Klein, D. R., Rosenberg, J. A., Brodbelt, J. S., & Eberlin, L. S. (2018).
263 Desorption Electrospray Ionization Mass Spectrometry Imaging of Proteins Directly from
264 Biological Tissue Sections. *Anal Chem, 90*(13), 7785-7789.
265 Gong, X., Zhao, Y., Cai, S., Fu, S., Yang, C., Zhang, S., & Zhang, X. (2014). Single cell analysis with
266 probe ESI-mass spectrometry: detection of metabolites at cellular and subcellular levels. *Anal*
267 *Chem, 86*(8), 3809-3816.
268 Guendel, A., Rolletschek, H., Wagner, S., Muszynska, A., & Borisjuk, L. (2018). Micro Imaging
269 Displays the Sucrose Landscape within and along Its Allocation Pathways. *Plant Physiol,*
270 *178*(4), 1448-1460.
271 He, Y., Guo, W., Luo, K., Sun, Q., Lin, Z., & Cai, Z. (2019). Poly-l-lysine-based tissue embedding
272 compatible with matrix-assisted laser desorption ionization-mass spectrometry imaging analysis
273 of dry and fragile aristolochia plants. *J Chromatogr A, 1608*, 460389.
274 Holst, S., Heijs, B., de Haan, N., van Zeijl, R. J., Briaire-de Bruijn, I. H., van Pelt, G. W., Mehta, A. S.,
275 Angel, P. M., Mesker, W. E., Tollenaar, R. A., Drake, R. R., Bovee, J. V., McDonnell, L. A., &
276 Wuhrer, M. (2016). Linkage-Specific in Situ Sialic Acid Derivatization for N-Glycan Mass

Spectrometry Imaging of Formalin-Fixed Paraffin-Embedded Tissues. *Anal Chem, 88*(11), 5904-5913.

Hu, J. B., Chen, Y. C., & Urban, P. L. (2013). Coffee-ring effects in laser desorption/ionization mass spectrometry. *Anal Chim Acta, 766*, 77-82.

Jensen, J. B., Peters, N. K., & Bhuvaneswari, T. V. (2002). Redundancy in Periplasmic Binding Protein-Dependent Transport Systems for Trehalose, Sucrose, and Maltose in Sinorhizobium meliloti. *Journal of Bacteriology, 184*(11), 2978-2986.

Li, B., Knudsen, C., Hansen, N. K., Jorgensen, K., Kannangara, R., Bak, S., Takos, A., Rook, F., Hansen, S. H., Moller, B. L., Janfelt, C., & Bjarnholt, N. (2013). Visualizing metabolite distribution and enzymatic conversion in plant tissues by desorption electrospray ionization mass spectrometry imaging. *Plant J, 74*(6), 1059-1071.

Li, B., Zhang, Y., Ge, J., Liu, K., & Li, P. (2018). Sample preparation for mass spectrometry imaging of leaf tissues: a case study on analyte delocalization. *Anal Bioanal Chem, 410*(28), 7449-7456.

Liao, Y., Fu, X., Zhou, H., Rao, W., Zeng, L., & Yang, Z. (2019). Visualized analysis of within-tissue spatial distribution of specialized metabolites in tea (Camellia sinensis) using desorption electrospray ionization imaging mass spectrometry. *Food Chem, 292*, 204-210.

Liu, Z., Lou, Z., Ding, X., Li, X., Qi, Y., Zhu, Z., & Chai, Y. (2013). Global characterization of neutral saccharides in crude and processed Radix Rehmanniae by hydrophilic interaction liquid chromatography tandem electrospray ionization time-of-flight mass spectrometry. *Food Chem, 141*(3), 2833-2840.

Lunsford, K. A., Peter, G. F., & Yost, R. A. (2011). Direct matrix-assisted laser desorption/ionization mass spectrometric imaging of cellulose and hemicellulose in Populus tissue. *Anal Chem, 83*(17), 6722-6730.

Nagy, G., Velickovic, D., Chu, R. K., Carrell, A. A., Weston, D. J., Ibrahim, Y. M., Anderton, C. R., & Smith, R. D. (2019). Towards resolving the spatial metabolome with unambiguous molecular annotations in complex biological systems by coupling mass spectrometry imaging with structures for lossless ion manipulations. *Chem Commun (Camb), 55*(3), 306-309.

Paine, M. R. L., Poad, B. L. J., Eijkel, G. B., Marshall, D. L., Blanksby, S. J., Heeren, R. M. A., & Ellis, S. R. (2018). Mass Spectrometry Imaging with Isomeric Resolution Enabled by Ozone-Induced Dissociation. *Angewandte Chemie International Edition, 57*(33), 10530-10534.

Paz-Alfaro, K. J., Ruiz-Granados, Y. G., Uribe-Carvajal, S., & Sampedro, J. G. (2009). Trehalose-mediated thermal stabilization of glucose oxidase from Aspergillus niger. *J Biotechnol, 141*(3-4), 130-136.

Peukert, M., Thiel, J., Peshev, D., Weschke, W., Van den Ende, W., Mock, H. P., & Matros, A. (2014). Spatio-temporal dynamics of fructan metabolism in developing barley grains. *Plant Cell, 26*(9), 3728-3744.

Pohnl, T., Schweiggert, R. M., & Carle, R. (2018). Impact of Cultivation Method and Cultivar Selection on Soluble Carbohydrates and Pungent Principles in Onions (Allium cepa L.). *J Agric Food Chem, 66*(48), 12827-12835.

Pokrzywnicka, M., & Koncki, R. (2018). Disaccharides Determination: A Review of Analytical Methods. *Crit Rev Anal Chem, 48*(3), 186-213.

Porta, T., Grivet, C., Kraemer, T., Varesio, E., & Hopfgartner, G. (2011). Single hair cocaine consumption monitoring by mass spectrometric imaging. *Anal Chem, 83*(11), 4266-4272.

Qu, L., Jiang, Y., Huang, X., Cui, M., Ning, F., Liu, T., Gao, Y., Wu, D., Nie, Z., & Luo, L. (2019). High-Throughput Monitoring of Multiclass Syrup Adulterants in Honey Based on the Oligosaccharide and Polysaccharide Profiles by MALDI Mass Spectrometry. *J Agric Food Chem, 67*(40), 11256-11261.

Sagara, T., Bhandari, D. R., Spengler, B., & Vollmann, J. (2020). Spermidine and other functional phytochemicals in soybean seeds: Spatial distribution as visualized by mass spectrometry imaging. *Food Sci Nutr, 8*(1), 675-682.

Sans, M., Feider, C. L., & Eberlin, L. S. (2018). Advances in mass spectrometry imaging coupled to ion mobility spectrometry for enhanced imaging of biological tissues. *Curr Opin Chem Biol, 42*, 138-146.

Shroff, R., Vergara, F., Muck, A., Svatos, A., & Gershenzon, J. (2008). Nonuniform distribution of glucosinolates in Arabidopsis thaliana leaves has important consequences for plant defense. *Proc Natl Acad Sci U S A, 105*(16), 6196-6201.

Takeo, E., Sugiura, Y., Uemura, T., Nishimoto, K., Yasuda, M., Sugiyama, E., Ohtsuki, S., Higashi, T., Nishikawa, T., Suematsu, M., Fukusaki, E., & Shimma, S. (2019). Tandem Mass Spectrometry Imaging Reveals Distinct Accumulation Patterns of Steroid Structural Isomers in Human Adrenal Glands. *Anal Chem, 91*(14), 8918-8925.

Velickovic, D., Chu, R. K., Carrell, A. A., Thomas, M., Pasa-Tolic, L., Weston, D. J., & Anderton, C. R. (2018). Multimodal MSI in Conjunction with Broad Coverage Spatially Resolved MS(2) Increases Confidence in Both Molecular Identification and Localization. *Anal Chem, 90*(1), 702-707.

Waldchen, F., Spengler, B., & Heiles, S. (2019). Reactive Matrix-Assisted Laser Desorption/Ionization Mass Spectrometry Imaging Using an Intrinsically Photoreactive Paterno-Buchi Matrix for Double-Bond Localization in Isomeric Phospholipids. *J Am Chem Soc, 141*(30), 11816-11820.

Xue, J., Liu, H., Chen, S., Xiong, C., Zhan, L., Sun, J., & Nie, Z. (2018). Mass spectrometry imaging of the in situ drug release from nanocarriers. *Sci Adv, 4*(10), eaat9039.

Ye, H., Gemperline, E., Venkateshwaran, M., Chen, R., Delaux, P. M., Howes-Podoll, M., Ane, J. M., & Li, L. (2013). MALDI mass spectrometry-assisted molecular imaging of metabolites during nitrogen fixation in the Medicago truncatula-Sinorhizobium meliloti symbiosis. *Plant J, 75*(1), 130-145.

Zhan, L., Xie, X., Li, Y., Liu, H., Xiong, C., & Nie, Z. (2018). Differentiation and Relative Quantitation of Disaccharide Isomers by MALDI-TOF/TOF Mass Spectrometry. *Anal Chem, 90*(3), 1525-1530.

Table of Contents graphic

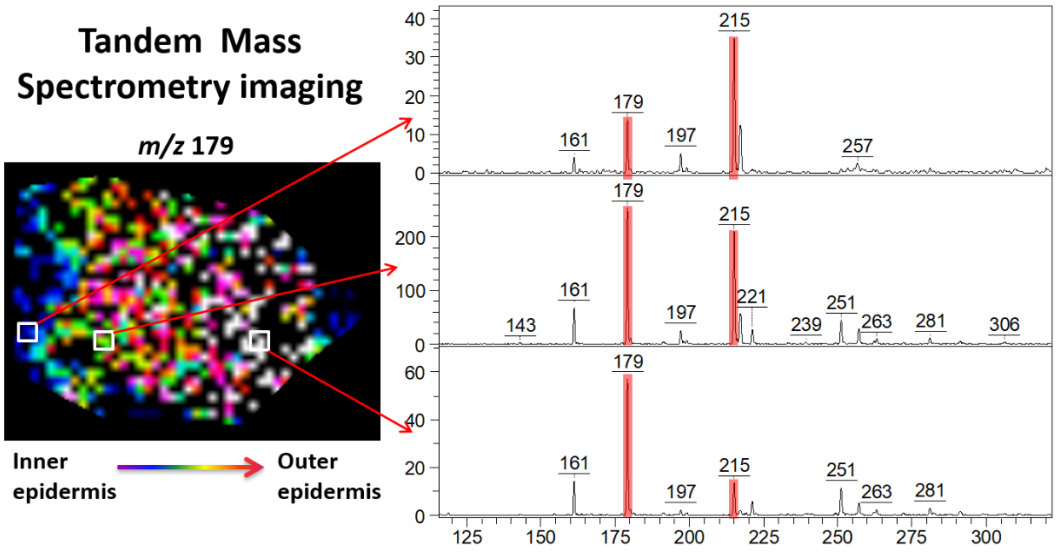

Highlights:

1. We develop a tandem mass spectrometry imaging method to visualize disaccharide isomers in plant tissues
2. Disaccharide isomers have different location in plant tissues
3. We found a new disaccharide isomer besides sucrose in onion bulbs